



# The Role of the Leading Edge Vortex in Lift Augmentation of Steadily Revolving Wings: A Change in Perspective

DOI:  
[10.1098/rsif.2017.0159](https://doi.org/10.1098/rsif.2017.0159)

**Document Version**  
Accepted author manuscript

[Link to publication record in Manchester Research Explorer](#)

**Citation for published version (APA):**  
Nabawy, M., & Crowther, B. (2017). The Role of the Leading Edge Vortex in Lift Augmentation of Steadily Revolving Wings: A Change in Perspective. *Journal of the Royal Society Interface*, 14(132), 0. <https://doi.org/10.1098/rsif.2017.0159>

**Published in:**  
Journal of the Royal Society Interface

**Citing this paper**  
Please note that where the full-text provided on Manchester Research Explorer is the Author Accepted Manuscript or Proof version this may differ from the final Published version. If citing, it is advised that you check and use the publisher's definitive version.

**General rights**  
Copyright and moral rights for the publications made accessible in the Research Explorer are retained by the authors and/or other copyright owners and it is a condition of accessing publications that users recognise and abide by the legal requirements associated with these rights.

**Takedown policy**  
If you believe that this document breaches copyright please refer to the University of Manchester's Takedown Procedures [<http://man.ac.uk/04Y6Bo>] or contact [uml.scholarlycommunications@manchester.ac.uk](mailto:uml.scholarlycommunications@manchester.ac.uk) providing relevant details, so we can investigate your claim.



# INTERFACE

## The Role of the Leading Edge Vortex in Lift Augmentation of Steadily Revolving Wings: A Change in Perspective

Journal:	<i>Journal of the Royal Society Interface</i>
Manuscript ID	rsif-2017-0159.R2
Article Type:	Perspective
Date Submitted by the Author:	23-Jun-2017
Complete List of Authors:	Nabawy, Mostafa; The University of Manchester, School of Mechanical, Aerospace and Civil Engineering Crowther, William; The University of Manchester, Mechanical, Aerospace and Civil Engineering
Categories:	Life Sciences - Engineering interface
Subject:	Biomechanics < CROSS-DISCIPLINARY SCIENCES, Biomimetics < CROSS-DISCIPLINARY SCIENCES
Keywords:	insect flight, leading edge vortex, aerodynamics, revolving wings, flapping flight, absence of stall

SCHOLARONE™  
Manuscripts

Only

1  
2  
3  
4  
5  
6  
7  
8  
9  
10  
11  
12

# The Role of the Leading Edge Vortex in Lift Augmentation of Steadily Revolving Wings: A Change in Perspective

Mostafa R. A. Nabawy\* and William J. Crowther

School of Mechanical, Aerospace and Civil Engineering, The University of Manchester,  
Manchester, M13 9PL, UK

\*Corresponding Author:

13  
14  
15  
16  
17  
18  
19  
20  
21  
22  
23  
24  
25  
26  
27  
28  
29  
30  
31  
32  
33  
34  
35  
36  
37  
38  
39  
40  
41  
42  
43  
44  
45  
46  
47  
48  
49  
50  
51  
52  
53  
54  
55  
56  
57  
58  
59  
60

Mostafa R A Nabawy  
E2 Pariser Building, Sackville Street,  
School of Mechanical, Aerospace and Civil Engineering,  
The University of Manchester,  
Manchester, M13 9PL, UK.  
Email: [mostafa.ahmednabawy@manchester.ac.uk](mailto:mostafa.ahmednabawy@manchester.ac.uk)

## Abstract

The presence of a stable Leading Edge Vortex (LEV) on steadily revolving wings increases the maximum lift coefficient that can be generated from the wing and its role is important to understanding natural flyers and flapping wing vehicles. In this paper, the role of LEV in lift augmentation is discussed under two hypotheses referred to as ‘additional lift’ and ‘absence of stall’. The ‘additional lift’ hypothesis represents the traditional view. It presumes that an additional suction/circulation from the LEV increases the lift above that of a potential flow solution. This behaviour may be represented through either the ‘Polhamus leading edge suction’ model or the so-called ‘trapped vortex’ model. The ‘absence of stall’ hypothesis is a more recent contender that presumes that the LEV prevents stall at high angles of attack where flow separation would normally occur. This behaviour is represented through the so-called ‘normal force’ model. We show that all three models can be written in the form of the same potential flow kernel with modifiers to account for the presence of a LEV. The modelling is built on previous work on quasi-steady models for hovering wings such that model parameters are determined from first principles, which allows a fair comparison between the models themselves, and the models and experimental data. We show that the two models which directly include the LEV as a lift generating component are built on a physical picture that does not represent the available experimental data. The simpler ‘normal force’ model, which does not explicitly model the LEV, performs best against data in the literature. We conclude that under steady conditions the LEV as an ‘absence of stall’ model/mechanism is the most satisfying explanation for observed aerodynamic behaviour.

**Key words:** insect flight, leading edge vortex, aerodynamics, revolving wings, flapping flight, absence of stall.

# 1. Introduction

## 1.1. Background

The aim of this paper is to provide a contribution to the debate on the role of the Leading Edge Vortex (LEV) in lift production in revolving wings based on rigorous comparison of low order modelling predictions with relevant experimental and numerical data. Whilst high order Computational Fluid Dynamics (CFD) methods are now able to accurately tackle flapping wing flows, the value of low order analytical models remains in that they provide insight into the flow physics that are not available from higher order methods. The existence of a LEV on insect like wings at low Reynolds numbers and the improvement in overall lift production associated with its presence is considered scientific fact [1-5]. However, there remain significant differences in opinion as to the *actual mechanism by which the lift is enhanced*. We group the different views on the role of the LEV in lift production under two hypotheses, namely the ‘additional lift’ hypothesis and the ‘absence of stall’ hypothesis. In the additional lift view, the additional circulation/suction from the LEV increases the lift above that of the nominal potential flow solution. In the absence of stall view, the LEV allows the flow to approximate the potential flow solution at high angles of attack at which the flow would normally be fully separated in a flow without a LEV.

Given the two hypotheses above, why does it matter which is more representative of the physics if the final outcome is the same? The reason is that the role of the LEV fundamentally affects the way we understand how insect-like wings at low Reynolds number work and hence our experimental approach to understanding insect flight and the design of engineered flapping wing vehicles. The choice also clearly affects our selection of models to represent the flow. If the ‘additional lift’ hypothesis is true then we should expect our models to explicitly include terms for lift due to a circulation contribution from the LEV. There is, of course, a third alternative in

1  
2  
3 that neither hypothesis is true, or that the actual situation is a combination of both, depending on  
4 the exact conditions. Nonetheless, the activity of trying to assess the validity of the different  
5 hypotheses remains instructive in that it provides structure to the debate which we believe is  
6 helpful.  
7  
8  
9  
10  
11

12  
13 Whilst the context for the work is flapping wing aerodynamics, it is important to stress we  
14 explicitly focus here on quasi-steady revolving wing aerodynamics. This in itself may be  
15 considered contentious if the LEV is assumed to be an unsteady phenomenon and hence cannot  
16 be fully captured by steady aerodynamic models. Indeed, if we allow unsteady effects, then in  
17 addition to the LEV as ‘additional lift’ and ‘absence of stall’ hypotheses, we could include a  
18 further hypothesis as LEV as ‘all the lift’ in which a wing with no bound circulation  
19 instantaneously traps a vortex and generates a finite amount of lift. We take the view that the  
20 quasi-steady assumption is both valid and useful. The quasi-steady assumption greatly reduces  
21 the size of the parameter space and there is a significant body of CFD and experimental work to  
22 which theory can be compared. It is understood that there will be unsteady effects due to stroke  
23 reversal in reciprocating rather than revolving motion. However, for the most important case of  
24 normal hovering with symmetric half-strokes, these effects are relatively small compared to the  
25 quasi-steady effects. Hence, with some caution, the arguments developed here for revolving  
26 motion retain core relevance when transferred to reciprocating motion.  
27  
28  
29  
30  
31  
32  
33  
34  
35  
36  
37  
38  
39  
40  
41  
42  
43  
44

45  
46 Finally, as a comment on the research method adopted in this paper, we recognise that use of  
47 low order models calibrated against experimental or CFD data clearly cannot be used to infer  
48 structure in the data from which they are calibrated. In the present work we thus adopt a first  
49 principles modelling approach based on the authors previous work in which model parameters  
50 are built up from geometry, kinematics and physics. These models are then properly predictive in  
51  
52  
53  
54  
55  
56  
57  
58  
59  
60

the sense that they may reasonably be used for predicting results for which experimental data does not exist. We now provide a more detailed technical description of the LEV and the current state of knowledge.

## 1.2. The Leading Edge Vortex (LEV)

A LEV is known to form on thin wings with moderate aspect ratio ( $\sim 3$ ), steadily revolving at high angles of attack and low Reynolds number of  $O(10^4)$  or lower, Fig. 1. The LEV is stable in that its location remains near the leading edge and it does not grow with time; this allows the flow over the upper surface of the wing to separate at the leading edge but then reattach before the trailing edge, Fig. 1a. A wing with a stable LEV is thus able to satisfy the Kutta condition at the trailing edge at angles of attack beyond which classical stall would occur for wings where no LEV is present, and consequently a substantial enhancement of the wing lift coefficient is achieved [1].

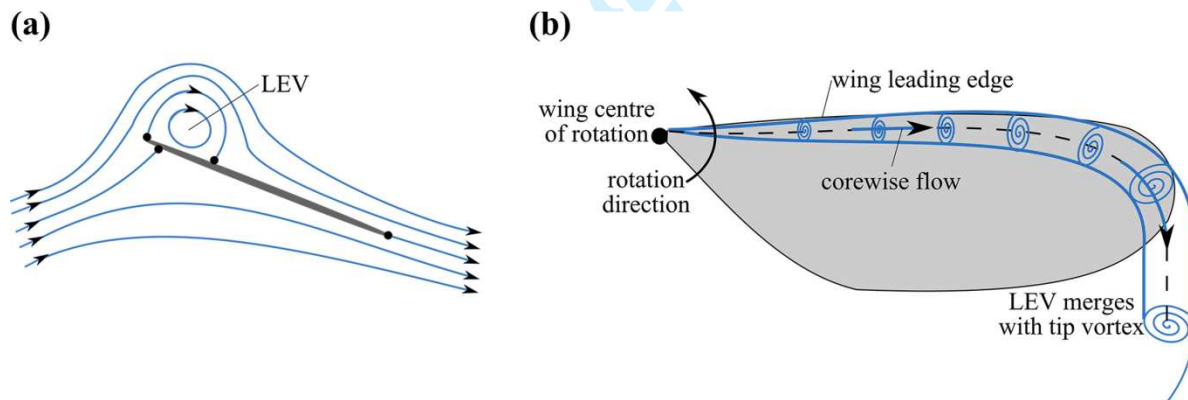


**Figure 1:** (a) Schematic showing the simplest valid leading edge vortex (LEV) structure for a cylindrical vortex - cross section view. The LEV is stable at high angles of attack with flow reattachment on the upper surface and satisfaction of the Kutta condition at the trailing edge. The black dots represent stagnation points. (b) An idealised top view schematic illustrating a conical LEV topology for a steadily revolving wing with a focus at the root. This topology has been observed at Reynolds numbers of  $O(10^3$  to  $10^4)$  [2,3].

1  
2  
3  
4  
5  
6  
7  
8  
9  
10  
11  
12  
13  
14  
15  
16  
17  
18  
19  
20  
21  
22  
23  
24  
25  
26  
27  
28  
29  
30  
31  
32  
33  
34  
35  
36  
37  
38  
39  
40  
41  
42  
43  
44  
45  
46  
47  
48  
49  
50  
51  
52  
53  
54  
55  
56  
57  
58  
59  
60

There has been substantial research within the last two decades directed at understanding the aerodynamic characteristics of revolving and flapping wings at Reynolds numbers relevant to insect/vertebrate flight. Some of these studies concentrated on flow visualisation to identify the flow topology, analyse circulation characteristics and determine possible causes for the stability of the LEV [2-14], whilst others concentrated on measuring the generated forces for different wing morphologies and kinematics [15-22]. Note that for completeness we refer to both steady and unsteady studies here. The identified LEV topologies were shown to vary from a conical form with a substantial spanwise flow at the vortex core (as that observed on model hawkmoth wings at Reynolds number from  $10^3$  to  $10^4$  [2], Fig. 1b) to a cylindrical form with a substantially weaker corewise vortex flow (as that observed on fruit fly and thrip wings at Reynolds number of the order  $10^2$  and  $10^1$  [3,4]). However, these differences in the LEV flow topologies were not reflected in differences in the measured lift polars [1,16,23], suggesting that the LEV is playing an aerodynamic role that it is to some extent independent of its shape under quasi-steady conditions.

Pitt Ford and Babinsky [24] used the ‘trapped vortex’ model to investigate the relation between lift production and LEV formation in unsteady wing motions. They proposed that most of the lift is due to the circulation contained in the LEV rather than the bound vortex. This conclusion was based on a best fit approach conducted between the ‘trapped vortex’ model and their experimental measurements. However, their experimental measurements were for an unsteady *translating* wing case at 15 degrees angle of attack and hence the experimental conditions do not generally represent the revolving/flapping wing scenario. Nevertheless, together with a consortium of different groups, this work was followed by experimental measurements for unsteady motions of translating and revolving rectangular wings (both surging



1  
2  
3 and pitching) at 45 degrees angle of attack [25-27]. It was found that unlike the translational  
4 case, the revolving wing motion allowed an *attached* LEV to form on top of the wing. They also  
5  
6 found that this attached vortex did not result in significantly higher lift coefficient compared to  
7  
8 the detached vortex from the translating unsteady case [26]. This is different from the quasi-  
9  
10 steady cases where it is well established that the attached LEV in revolving motion allows  
11  
12 significantly higher lift coefficient values compared to the detached LEV in translational motion  
13  
14 (see for example Usherwood and Ellington [15], and Sane [1]). Later, Phillips *et al.* [28] adopted  
15  
16 the findings of Pitt Ford and Babinsky for unsteady translating wings, and calculated the lift  
17  
18 based on the circulation contained only within the formed LEV for a series of flapping wings  
19  
20 with different Rossby number (note that translating motion corresponds to infinite Rossby  
21  
22 number whilst revolving motion corresponds to a finite Rossby number value equivalent to the  
23  
24 ratio of the radius of gyration to the mean chord [19]). The LEV lift coefficient was found to  
25  
26 *increase* as the Rossby number increases [28], a result which is inconsistent with previous  
27  
28 experimental force measurements [19] and numerical simulation [29]. Thus, whilst unsteady  
29  
30 effects undoubtedly play an effect in establishing the flow field, the evidence for this in the  
31  
32 literature is incomplete.

33  
34  
35  
36  
37  
38  
39  
40  
41 The presence of a LEV was first identified by Maxworthy whilst conducting experiments on  
42  
43 the Weis-Fogh ‘clap and fling’ mechanism [30]. Subsequently, the role of the LEV in insect  
44  
45 aerodynamics was developed by Ellington and his group [2], who proposed the LEV as a  
46  
47 ‘dynamic/delayed stall’ mechanism. This description has persisted despite that fact that dynamic  
48  
49 stall is an unsteady mechanism that cannot be maintained for an indefinite period and that the  
50  
51 vortex created during a dynamic stall convects directly after the wing starts to translate [31,32,3].  
52  
53 Furthermore, many revolving wing experiments [15-23] demonstrated that the LEV is a *steady*  
54  
55  
56  
57  
58  
59  
60

1  
2  
3 aerodynamic mechanism that can be maintained indefinitely on revolving wings. Recently, Kruyt  
4  
5 *et al.* [33] experimentally demonstrated that stall is prevented on revolving wings as long as they  
6  
7 have an aspect ratio (defined from centre of revolution) that does not exceed four, a number that  
8  
9 most insects and hummingbirds wings are clustered around.  
10  
11

## 12 13 14 15 **2. Models**

### 16 **2.1 Overview**

17  
18 In this section we introduce three low order models that have previously been used to model  
19  
20 steady wing flows, namely the ‘normal force’ model, the ‘leading edge suction’ model and the  
21  
22 ‘trapped vortex’ model. A contribution of this section is to show that all three of these models  
23  
24 can be expressed in the form of a common potential flow model corrected for three dimensional  
25  
26 effects, plus additional model specific corrections to account for operation at high angle of attack  
27  
28 or the addition of vortex lift. The fact that these apparently dissimilar models can all be  
29  
30 expressed with a common core allows attention to be focussed on the physical contribution of the  
31  
32 leading edge vortex in the model. We first present the potential flow model which provides the  
33  
34 core of the three models under consideration.  
35  
36  
37  
38  
39

### 40 41 **2.2 Potential flow model**

42  
43 The classical potential flow model is based on assumption of fully attached flow to the wing up  
44  
45 to 90 degrees angle of attack. In an idealised 2d flow, the lift coefficient,  $C_l$ , for a flat plate is  
46  
47 expressed as:  
48  
49

$$50 \quad C_l = 2\pi \sin \alpha = C_{l\alpha,2d} \sin \alpha . \quad (1)$$

51  
52  
53  
54  
55  
56  
57  
58  
59  
60

where,  $C_{l\alpha,2d}$  is the 2d aerofoil lift curve slope and  $\alpha$  is the angle of attack. For a 3d wing, the lift coefficient,  $C_L$ , is therefore expressed as:

$$C_L = C_{L\alpha,3d} \sin \alpha = (C_{l\alpha,2d} \sin \alpha \cos \alpha) \sec \alpha . \quad (2)$$

where,  $C_{L\alpha,3d}$  is the 2d lift curve slope corrected for appropriate geometry and kinematic effects (see section 2.6). Note that the right hand side of Eqn. 2 is written in this form to provide basis of comparison with the ‘normal force’ model that will be discussed later. The potential flow model is useful at low angles of attack, but clearly non-physical at high angles of attack approaching 90 degrees, where geometry dictates that the lift must tend towards zero when the wing is perpendicular to the flow.

### 2.3. Normal force model

The 2d form of normal force model is expressed as the potential flow model multiplied by a  $\cos \alpha$  term [34,35]:

$$C_l = \pi \sin 2\alpha = \frac{C_{l\alpha,2d}}{2} \sin 2\alpha = C_{l\alpha,2d} \sin \alpha \cos \alpha . \quad (3)$$

Consequently from Eqn. 3, the 3d wing form is expressed as:

$$C_L = C_{L\alpha,3d} \sin \alpha \cos \alpha . \quad (4)$$

The  $\cos \alpha$  term may be thought of as a geometric correction to the potential flow model that drives the lift to zero at 90 degrees angle of attack as required by physics. The model structure of Eqn. 4 written in terms of a normal force coefficient,  $C_N$ , is:

$$\begin{aligned}
 C_N &= \hat{C}_N \sin \alpha, \\
 C_L &= C_N \cos \alpha, \\
 C_D &= C_N \sin \alpha.
 \end{aligned}
 \tag{5}$$

where,  $\hat{C}_N$  is the normal force coefficient amplitude and  $C_D$  is the 3d wing drag coefficient. Thus the model implicitly assumes that the overall aerodynamic force is *normal* to the wing chord [15,18,36-41]. As an aside, this requires that: (1) the wing is an infinitesimally thin flat plate, and hence there is no chordwise component to the integrated surface pressure force, and (2) the chordwise tangential force due to skin friction is negligible compared to the integrated surface pressure force acting normal to the chord [18]. Note that the normal force model has historically been used to represent the un-stalled 2d aerofoil lift coefficient of wings operating at high angles of attack within the helicopter and fixed wing aerodynamics literature [34,35]. Later, various models based on the normal force assumption have been widely used to represent the quasi-steady aerodynamics of revolving/flapping wings [15,18,36-41].

## 2.4 Leading edge suction model

The leading edge suction model is based on the so-called ‘*leading edge suction analogy*’ proposed by Polhamus for delta wings [42]. The conical LEV created on laminar revolving/flapping wings is similar in form to the LEV observed over delta wings at subsonic speeds and high angles of attack. This prompted several researchers [1,15,41,43] to use the ‘leading edge suction’ model for delta wings to analyse the revolving/flapping wing problem. Note that whilst at first sight revolving/flapping wings and steady delta wings appear quite different, the key similarity is that in each a stable LEV is able to form. For the delta wing it is the leading edge sweep which provides the stabilising spanwise pressure gradient; for the flapping/revolving wing it is the spanwise velocity distribution that provides the stabilising

pressure gradient [19]. The ‘leading edge suction’ model is formulated on the basis that the leading edge flow separation that creates the LEV causes a loss of the leading edge suction that would have otherwise been generated had the flow remained attached at the leading edge. The lift is thus comprised of two components: The first is the potential flow lift but with zero leading edge suction. The second is a vortex lift related to the ‘missing’ leading-edge suction associated with the potential flow. Polhamus did not attempt to provide a theoretical proof of his analogy; however, it has historically proved useful in estimating aerodynamic force coefficients on delta wings within their normal operating range of angles of attack ( $\alpha \leq 25^\circ$ ). It is worth noting that this angle of attack limit is below the typical maximum angle of attack of around 45 degrees up to which insect wings operate. The model can be expressed for 3d wings as follows [42]:

$$C_L = \underbrace{C_{L\alpha,3d} \sin \alpha \cos^2 \alpha}_{\text{Potential lift, } C_{L,p}} + \underbrace{\left( C_{L\alpha,3d} - \frac{kC_{L\alpha,3d}^2}{\pi AR} \right) \frac{1}{\cos \Lambda} \sin^2 \alpha \cos \alpha}_{\text{Vortex lift, } C_{L,v}}, \quad (6)$$

where  $\Lambda$  is the wing sweep angle (which is assumed zero for revolving wings),  $AR$  is the wing aspect ratio and  $k$  is the so-called ‘ $k$ -factor’ included to correct for the difference in efficiency between assumed ideal uniform downwash distribution and real downwash distribution [44,45]. In order to make direct comparisons with other models of interest, we rearrange Eqn. 6 as follows:

$$C_L = \left( C_{L\alpha,3d} \sin \alpha \cos \alpha \right) \underbrace{\left( \cos \alpha + \left( 1 - \frac{k_{ind} k_{per} C_{L\alpha,3d}}{\pi AR} \right) \sin \alpha \right)}_{K_{Pol}(\alpha)}. \quad (7)$$

Note that to address the specific flow physics associated with revolving wings the  $k$ -factor is split into two components:  $k_{ind}$  to account for the non-uniform downwash effect and  $k_{per}$  to account

for wake periodicity. The method for prediction of these parameters is based on the authors' previous work which may be found in [44].

## 2.5 Trapped vortex model

Following the work of Saffman and Sheffield [46], the so-called 'trapped vortex model' is based on steady, inviscid, incompressible and irrotational 2d potential flow over a flat plate with an embedded free vortex. Thus the model has similarity to the leading edge suction model, however in this present case the strength of the LEV is a *free* variable. This model is based on the well-known Joukowski transformation approach where the flow is mapped from a circle of radius  $a$  to a flat plate with a chord length of  $4a$  inclined at an angle of attack  $\alpha$  to the free stream,  $U$  [46,24]. Briefly, a free vortex element is included with a circulation  $\Gamma_{free}$  located at  $\zeta = \rho e^{i\varphi}$  in the circle plane, where the radius  $\rho$  and the angle  $\varphi$  are user specified variables to define the free vortex location in the circle plane. An image vortex of equal but opposite sign to  $\Gamma_{free}$  is located at the inverse square point and a second vortex of equal circulation to  $\Gamma_{free}$  is located at the circle centre; thus, the circulations of image vortices cancel [24]. The Kutta condition is satisfied by equating the velocity to zero at  $\zeta = a$ . The magnitude of the bound circulation can be represented as [24]:

$$\Gamma = 4\pi a U \sin \alpha + \Gamma_{free} \frac{2a(a - \rho \cos \varphi)}{\rho^2 - 2a\rho \cos \varphi + a^2}. \quad (8)$$

The first term of the right hand side of Eqn. 8 is the well-known result for the bound circulation of a flat plate at incidence, whereas the second term accounts for the circulation added by the

1  
2  
3  
4 *trapped* free vortex (LEV) located at  $\zeta = \rho e^{i\varphi}$ . Expressing Eqn. 8 in terms of the 2d lift  
5  
6 coefficient gives:

$$C_l = \frac{\Gamma}{2aU} = 2\pi \sin \alpha + \underbrace{\frac{\Gamma_{free}}{2aU} \frac{2(1 - (\rho/a) \cos \varphi)}{(\rho/a)^2 - 2(\rho/a) \cos \varphi + 1}}_{C_{lfree,2d}} \quad (9)$$

14  
15 The addition of a free vortex in the above results represents an additional *constant* increment  
16  
17 in circulation at all angles of attack. Now, for a given chord,  $U$  and  $\alpha$ , Eqn. 9 becomes one  
18  
19 equation in three unknowns ( $C_l$ ,  $\Gamma_{free}$  and  $\zeta$ ); thus it cannot be used without further input to  
20  
21 evaluate the lift, and either additional information or experimental data (as in [24]) needs to be  
22  
23 used to define some of the unknown parameters. By analogy, Eqn. 9 can be written to express  
24  
25 the overall lift coefficient of the 3d wing as:

$$C_L = C_{L\alpha,3d} \sin \alpha + C_{Lfree,3d} \quad (10)$$

26  
27 Note that the first term in Eqn. 10 is the potential flow model as stated in Eqn. 2. This is to be  
28  
29 expected since the potential flow model is ultimately derived by the same Joukowski  
30  
31 transformation approach. The free vortex contribution to lift as defined by the second term in  
32  
33 Eqn. 10 will ultimately depend on the strength of the LEV as a function of angle of attack. From  
34  
35 fundamental considerations we know that the LEV strength will be zero at zero angle of attack  
36  
37 and will increase with increasing angle of attack. From observation we also know that there is a  
38  
39 limit to the size to which the LEV can grow as the angle of attack increases. Thus whilst we  
40  
41 cannot calculate values for the free vortex lift in Eqn. 10 directly, we can infer that if this vortex  
42  
43 lift is coming from the LEV, the contribution will increase with increasing angle of attack up to a  
44  
45 saturation limit after which it will remain approximately constant until dropping back to zero as  
46  
47 the LEV is shed completely from the leading edge.

## 2.6 Calculation of the 3d lift curve from first principles

All three models considered in this study are direct functions of the 3d wing lift curve slope at small angles of attack,  $C_{L\alpha,3d}$ . We evaluate  $C_{L\alpha,3d}$  based on the quasi-steady lifting line theory for hovering wings developed by the authors in [37]. The approach provides a good compromise between simplicity and accuracy for lift characterisation, and accounts for the necessary physical aspects required to correctly model a steadily revolving wing including: (1) velocity varying as a function of spanwise location; (2) wing planform shape effects including wing chord distribution and aspect ratio; (3) downwash corrections to account for non-uniformity of the developed downwash, and discreteness and periodicity in the wake; (4) corrections for small aspect ratio relevant to insect-like planforms. For more details of the theory, readers are referred to [37].

## 2.7 Comparison of model structures

Before comparing outputs of the three models presented above with experimental data we undertake an objective comparison of the implications of the different model structures. Figure 2 shows a graphical comparison of the models over the whole of the first quadrant of angle of attack ( $0 - 90^\circ$ ). Also shown here is a nominal experimental representation for a translating wing of the same planform without a LEV. We introduce here a number of transformations (or ‘effects’) in the  $C_L - \alpha$  space associated with well-established classical aerodynamics [47] that helps us relate differences in model behaviour. The first two effects relate to the 2d aerodynamic characteristics of the wing section. These are firstly, the ‘flap effect’, corresponding to a shift of a lift curve in a direction perpendicular to the lift curve at zero angle of attack, and secondly, the ‘slat effect’, corresponding to a translation of a lift curve in a direction parallel to the lift curve slope at zero angle of attack. The third effect is related to changes in the overall lift curve slope of the wing, for which planform is normally the driver. We will refer to this as a ‘planform



effect' as distinct from a 'section effect'. From a modelling point of view, the 'flap effect' is consistent with provision of an increment in circulation at all angles of attack whilst the 'slat effect' is consistent with an increase in circulation at angles of attack where the maximum lift coefficient,  $C_{L,max}$ , is limited by stall. Therefore, the 'flap effect' is associated with the 'trapped vortex' model, the 'slat effect' with the 'normal force' model, and the 'planform effect' (between  $0 \leq \alpha \leq 45^\circ$ ) with the 'leading edge suction' model.

$$\begin{array}{ll}
 \text{Potential flow model} & C_L = C_{L\alpha,3d} \sin\alpha \\
 \text{Normal force model} & C_L = C_{L\alpha,3d} \sin\alpha \cos\alpha \\
 \text{Leading edge suction model} & C_L = C_{L\alpha,3d} \sin\alpha \cos\alpha K_{Pol}(\alpha) \\
 \text{Trapped vortex model} & C_L = C_{L\alpha,3d} \sin\alpha + C_{Lfree,3d}
 \end{array}$$

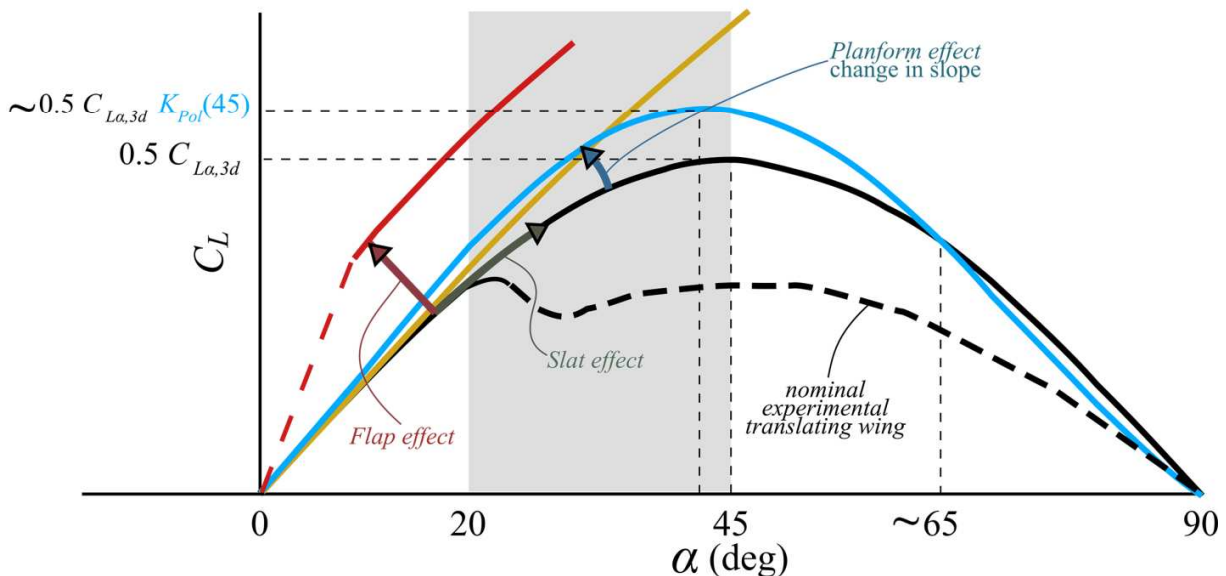


**Figure 2:** Comparison of the mathematical structure and graphical representation for the models discussed in this study over the first quadrant of angle of attack (potential flow (yellow), normal force (black), leading edge suction (blue) and trapped vortex with  $C_{Lfree,3d} > 0$  (red)). All models contain the potential flow model as a component. We choose to show the potential flow model results only up to  $45^\circ$  since this model is known to be non-physical as it approaches  $90^\circ$  angle of attack. Gray band represents typical angle of attack values within the mid half-strokes of normal hovering insect flight. A nominal experimental representation of a classical stalled translating wing (dashed line) is added for reference.

## 2.8 Compatibility of models with observed wing pressure distributions

The focus of the present work is on prediction of integrated aerodynamic loads on wings; however, it is also fair to ask to what extent the various models are compatible with the load distributions observed from CFD studies, e.g. [48]. In particular, pressure data shows that under some flow conditions there is evidence of a suction foot print consistent with that expected from an attached vortex at the leading edge. Given this, we recognise that it is reasonable to expect that the suction from the LEV is directly responsible for at least some of the lift being generated by the wing. However, it seems that the suction footprint is only evident inboard and is relatively small in chordwise extent (see figures 15 and 20 from [48]) and hence in this case the integrated contribution to overall lift is expected to be minor.

## 3. Comparison of Model Predictions with Experimental and Numerical Data

### 3.1 The revolving wing experiment

Before comparing the models to the revolving wing experiment results, we will discuss some essential aspects of the experimental methods used in the literature. Revolving wing experiments are routinely used to simulate flapping wings during the mid half-stroke wing translational phase. The revolving wing set-up is useful in that it preserves the main steady aerodynamic features of an insect-like flapping wing during mid half-stroke including the spanwise velocity and pressure gradients as well as the induced effects due to tip vortices. However, it does not capture unsteady aerodynamic effects due to stroke reversals and/or wing-wing interactions that may be important. Nevertheless, the translational aerodynamic mechanism (simulated by the revolving wing set-up) is sufficient to account for weight support production in hovering [15,18,41,49,50]. Eight revolving wing cases from the literature are considered here, see Table 1. Three different data

sets (from three different research groups) are used for the hawkmoth; one data set is used for each of the bumble bee, the mayfly, the fruitfly, the pigeon, and the hummingbird. The wing planforms are defined through the relevant shape parameters: the single wing aspect ratio,  $AR$ , and the non-dimensional radius of the first and second moments of wing area, ( $\hat{r}_1$  and  $\hat{r}_2$  respectively) [51-53,37], which for insect wings are strongly correlated through the relation:

$$\hat{r}_1 = 1.106\hat{r}_2^{1.366} [53].$$

**Table 1:** Definition of geometric, experimental, and analytical parameters for the datasets used to evaluate LEV models.

Species	Wing Description					Measurement conditions		Analytical Values	
	$AR$	$\hat{r}_1^*$	$\hat{r}_2$	$t/\bar{c}$ (%)	Material	Measurement Interval	Re	$C_{L\alpha,3d}$	$K_{Pol}(\alpha = 45^\circ)$
<b>Hawkmoth HM1 [15]</b>	2.83	0.44	0.511	< 1.6	Stiffened Plastic	180° - 450°	8071	2.742	1.15
<b>Hawkmoth HM2 [21]</b>	3.09	0.44	0.511*	3.7	Acrylic	90° - 270°	6800	2.863	1.16
<b>Hawkmoth HM3 [22]</b>	2.78	0.44	0.511*	2	Rigid-CFD	1080° - 1440°	5400	2.717	1.15
<b>Bumble bee BB [16]</b>	3.16	0.477	0.541	-	Stiffened Plastic*	180° - 450°	5496	2.813	1.16
<b>Mayfly MF [16]</b>	3.21	0.484	0.546	5	Stiff card	-	1100	2.816	1.16
<b>Fruitfly FF [18,19]</b>	3.3*	0.54	0.59*	~3*	Acrylic	Arc of 320°	~110	2.677	1.17
<b>Pigeon [17]</b>	3.21	0.443	0.512	2.8*	Card	-	54000	2.91	1.16
<b>Hummingbird HB [20]</b>	4.069	0.43	0.499	-	Real wing	-	9800	3.239	1.2

\*estimated.

With the exception of the hummingbird wing, the wing section used was an un-cambered flat plate. The thickness to mean chord ratio ( $t/\bar{c}$ ) varies between 1.6 and 5 %. Whilst this will have an effect on the zero lift drag coefficient,  $C_{D0}$ , the effect on lift coefficient (which is the focus of the present study) is minor. The material used to manufacture each wing is also provided in Table 1. This allows qualitative judgement on the degree of rigidity of the used wing models.

1  
2  
3 Whilst all experiments (with the exception of the hummingbird case) assumed rigid wings, this  
4 assumption was not perfectly achieved in reality. This can be seen from the non-zero lift values  
5 at 90° angle of attack (see Fig. 3). For the hummingbird case, both compliance and camber  
6 effects are expected to have affected the measurements; however, these effects are more  
7 pronounced at the very high angle of attack range (i.e.  $\alpha > 45^\circ$ ). Thus, we find this a still useful  
8 case for comparison particularly for the typical operation angle of attack values up to 45°.  
9  
10  
11  
12  
13  
14  
15  
16

17  
18 An issue with the available experimental data is the inconsistency of the angular measurement  
19 interval provided in Table 1. The angular measurement interval corresponds to the wing  
20 revolution sector within which the measurement data were collected. Revolving wings may  
21 experience a change in the aerodynamic force coefficient values after the first revolution when  
22 the wing passes through the disturbed air from the first revolution [22,54]. Additionally, the  
23 validity of angular measurement of revolving wing experiments is bounded by the need to allow  
24 starting effects to diminish. Whilst absolute values of force coefficients are affected by non-ideal  
25 conditions, it is understood that variation of values with angle of attack is relatively unaffected.  
26 Hence, with some caution, the lack of consistency in experimental conditions between the  
27 validation studies is manageable.  
28  
29  
30  
31  
32  
33  
34  
35  
36  
37  
38  
39

40  
41 The measurement Reynolds number,  $Re$ , for each experimental set-up is also provided in  
42 Table 1. These range from  $O(10^2)$  to  $O(10^4)$ . Experiments [16,19,23] have demonstrated that the  
43 dependence of lift coefficient on the Reynolds number in this range is small. A CFD simulation  
44 [22] has confirmed this for a higher range of Reynolds number bound up to the  $O(10^5)$ . On the  
45 other hand, Reynolds number does affect the zero lift drag coefficient value,  $C_{D0}$  [19,23]. For  
46 revolving wings operating at moderate to high incidence, the relation:  
47  
48  
49  
50  
51  
52  
53  
54  
55  
56  
57  
58  
59  
60  
$$C_D = C_{D0} + C_L \tan(\alpha)$$
 provides a satisfactory drag coefficient representation. For  $Re O(10^3)$  and

1  
2  
3 above,  $C_{D0}$  is practically negligible; however, when  $Re$  is of the  $O(10^2)$ ,  $C_{D0}$  seems to have a  
4  
5  
6 value around 0.4 [16,18,19,23,38,40].  
7  
8

### 9 10 **3.2 Comparison of models with revolving wing data**

11 Figure 3 compares the calculated lift coefficient variation from the modelling approaches  
12 presented in Section 2 within the first quadrant of angle of attack for the eight wing cases. When  
13 reviewing the data in Fig. 3 it should be noted that for normal hovering flight the typical values  
14 for the mid half-stroke angles vary between 20 and 45 degrees [37]. The average errors for the  
15 normal force, the leading edge suction, and the potential flow models compared to the  
16 experimental data in this angle of attack range are 11%, 31%, and 33%, respectively.  
17  
18  
19  
20  
21  
22  
23  
24  
25  
26  
27  
28  
29  
30  
31  
32  
33  
34  
35  
36  
37  
38  
39  
40  
41  
42  
43  
44  
45  
46  
47  
48  
49  
50  
51  
52  
53  
54  
55  
56  
57  
58  
59  
60

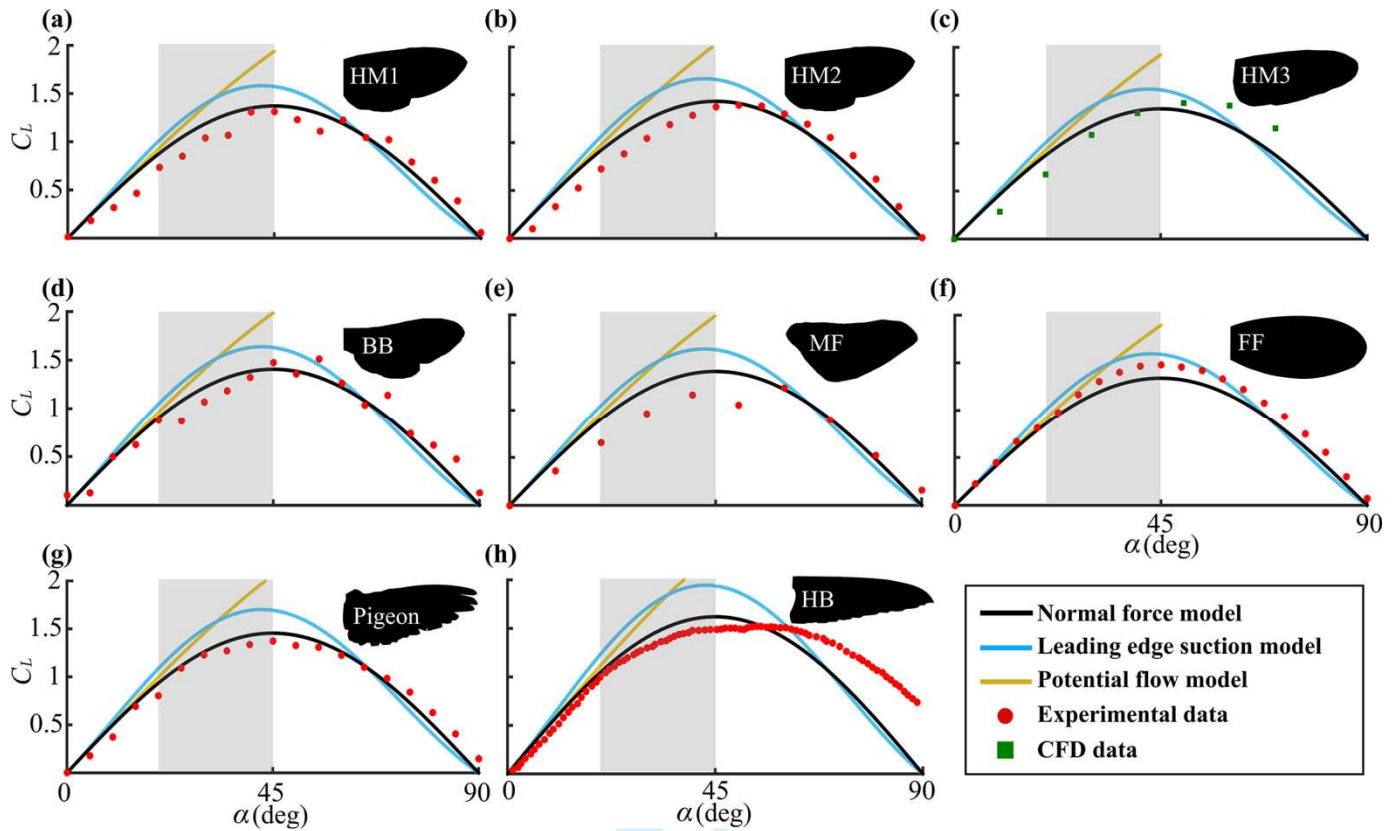


**Figure 3:** Comparison of aerodynamic model predictions against experimental and CFD data. Lift coefficient data is plotted against geometric angle of attack. Models are compared to available data for (a) Hawkmoth-1; experimental data digitised from figure 6 of [15], (b) Hawkmoth-2; experimental data digitised from figure 5 of [21], (c) Hawkmoth-3; CFD data digitised from figure 5 of [22], (d) Bumble bee; experimental data digitised from figure 7 of [16], (e) Mayfly; experimental data digitised from figure 8 of [16], (f) Fruitfly; experimental data digitised from figure 7 of [19], (g) Pigeon; experimental data digitised from figure 3 of [17], and (h) Hummingbird; experimental data digitised from figure 6 of [20].

Values of  $C_{L\alpha,3d}$  for the eight cases considered in this study are provided in Table 1. The

leading edge suction model requires further inputs for the values of the  $k$ -factor contributors  $k_{ind}$  and  $k_{per}$  within the  $K_{Pol}$  term (see Eqn. 7). Values of  $k_{ind}$  are based on the approach proposed by the authors in [44]. As for  $k_{per}$ , a constant value of 1.1 is assumed for all species considered here. This is based on a previous conclusion that variation of the wake periodicity  $k$ -factor is minimum and its value is usually clustered around 1.1 [44,51].

#### 4. Discussion

The comparison of models against experimental and numerical data presented in Fig. 3 shows that the ‘normal force’ model provides the best fit with respect to both the shape of variation and the amplitude. The ‘leading edge suction’ model provides a fair fit with respect to the shape of variation of lift against angle of attack; however, it over-estimates the lift magnitudes up to an angle of attack value around  $65^\circ$  and then starts to under-estimate it. It is noteworthy that the potential lift component of the ‘leading edge suction’ model,  $C_{L,p}$ , is a further attenuation of the potential lift, i.e.  $C_{L,p} = \text{Normal Force Model} \times \cos \alpha$ . The  $\cos^2 \alpha$  in the  $C_{L,p}$  term was explained by Polhamus to arise from the assumption of a Kutta-type flow condition at the leading edge [55]. However, the application of a Kutta condition at the leading edge was shown to be mathematically invalid by Saffman and Sheffield [46]. This attenuation of the potential lift was compensated for by the addition of vortex lift,  $C_{L,v}$ ; hence allowing recovery of the total lift coefficient value.

The total lift coefficient of the leading edge suction analogy for the angles of attack between  $0^\circ$  and  $45^\circ$  can be regarded as effectively having a higher lift curve slope compared to the ‘normal force’ model. The difference between the two models is explained with the help of the  $K_{Pol}$  term. As shown in Table 1, the  $K_{Pol}$  term attains values ranging between 1.15 and 1.2 at  $\alpha = 45^\circ$  meaning around a 15-20% increase in amplitude compared to the ‘normal force’ model. It should be noted that the Polhamus model is known to over-predict the wing lift coefficient as the wing aspect ratio increases beyond 1.5. Very good agreement between the Polhamus model and delta wing experimental data of aspect ratios up to 1.5 was shown; however, for an aspect ratio of two, the model over-predicted the experimental lift coefficient values [42]. In addition, the ‘leading



1  
2  
3 edge suction' model was only assessed within the typical operation angle of attack range for  
4  
5 delta wings ( $\alpha \leq 25^\circ$ ) and its accuracy within the higher angle of attack regime ( $25^\circ < \alpha \leq 45^\circ$ )  
6  
7 was not considered. Therefore, for the wing aspect ratios and angles of attack considered, this  
8  
9 difference between the 'leading edge suction' and 'normal force' models is not unexpected.  
10  
11

12  
13 The potential flow model (i.e. 'trapped vortex' model with zero LEV circulation strength)  
14  
15 results in Fig. 3 become increasingly non physical at high angles of attack as the model predicts  
16  
17 maximum lift at 90 degrees angle of attack whereas the observed lift is zero. However, the model  
18  
19 offers good prediction of lift up to around  $20^\circ$  angle of attack, after which it starts to  
20  
21 unacceptably over-predict the measurement data. Referring back to Eqn. 2, it can be seen that at  
22  
23  $45^\circ$  angle of attack (where the maximum practical lift coefficient is expected to occur) the  
24  
25 potential flow model over-predicts the 'normal force' model by a factor of  $\sqrt{2}$  (i.e. 41.4%  
26  
27 increase in lift coefficient). Despite these concerns, the important result here is that by setting  
28  
29  $C_{L,free,3d}$  to zero in the 'trapped vortex' model, the model still *over-predicts* the lift coefficient.  
30  
31 Hence additional circulation from the leading edge vortex is not required to predict the observed  
32  
33 lift coefficient values.  
34  
35  
36  
37  
38

39  
40 In conclusion, of the models evaluated, the 'normal force' model provides the best correlation  
41  
42 with measured lift values from steadily revolving wings experiencing a LEV, despite the fact that  
43  
44 it does not account for additional circulation due to the LEV as in the 'trapped vortex' model, or  
45  
46 account for a vortex lift (suction) component as in the Polhamus model. This shows that it is  
47  
48 unnecessary to add a specific lift contribution from the LEV to explain the high lift generated in  
49  
50 the experimental results. Thus from the two initial hypotheses for the effect of the LEV on lift,  
51  
52 we find that improvement in performance via 'absence of stall' is a more satisfying explanation  
53  
54 than 'additional lift'.  
55  
56  
57  
58  
59  
60



**Data accessibility:**

This article has no additional data.

**Authors' Contributions:**

MN conceived the work, MN and WC developed the models, analysed the results and wrote the paper.

**Competing Interests:**

We declare we have no competing interests.

**Funding:**

No funding has been received for this article.

**References**

1. Sane, S.P. 2003 The aerodynamics of insect flight. *J. Exp. Biol.* **206**: 4191-4208. (doi 10.1242/jeb.00663)
2. Ellington, C.P., van den Berg, C., Willmott, A.P., Thomas, A.L.R. 1996 Leading-edge vortices in insect flight. *Nature* **384**: 626-630. (doi 10.1038/384626a0)
3. Shyy, W., Liu, H. 2007 Flapping wings and aerodynamic lift: the role of leading-edge vortices. *AIAA J.* **45**, 2817-2819. (doi 10.2514/1.33205)
4. Birch, J.M., Dickinson, M.H. 2001 Spanwise flow and the attachment of the leading edge vortex on insect wings. *Nature* **412**: 729-733. (doi 10.1038/35089071)
5. Birch, J.M., Dickson, W.B., Dickinson, M.H. 2004 Force production and flow structure of the leading edge vortex on flapping wings at high and low Reynolds numbers. *J. Exp. Biol.* **207**: 1063-1072. (doi 10.1242/jeb.00848)
6. Lentink, D., Dickson, W.B., Van Leeuwen, J.L., Dickinson, M.H. 2009 Leading-edge vortices elevate lift of autorotating plant seeds. *Science* **324**: 1438-1440. (doi 10.1126/science.1174196)
7. Bomphrey, R.J., Lawson, N.J., Harding, N.J., Taylor, G.K., Thomas, A.L. 2005 The aerodynamics of *Manduca sexta*: digital particle image velocimetry analysis of the leading-edge vortex. *J. Exp. Biol.* **208**: 1079-1094. (doi 10.1242/jeb.01471)
8. Bomphrey, R.J., Lawson, N.J., Taylor, G.K., Thomas, A.L.R. 2006 Application of digital particle image velocimetry to insect aerodynamics: measurement of the leading-edge vortex and near wake of a Hawkmoth. *Exp. Fluids* **40**: 546-554. (doi 10.1007/s00348-005-0094-5)
9. Bomphrey, R.J., Taylor, G.K., Thomas, A.L.R. 2009 Smoke visualization of free-flying bumblebees indicates independent leading edge vortices on each wing pair. *Exp. Fluids* **46**: 811-821. (doi 10.1007/s00348-009-0631-8)
10. Warrick, D.R., Tobalske, B.W., Powers, D.R. 2005 Aerodynamics of the hovering hummingbird. *Nature* **435**: 1094-1097. (doi 10.1038/nature03647)
11. Warrick, D.R., Tobalske, B.W., Powers, D.R. 2009 Lift production in the hovering hummingbird. *P. Roy. Soc. Lond. B Bio.* **276**: 3747-3752. (doi 10.1098/rspb.2009.1003)

12. Muijres, F.T., Johansson, L.C., Barfield, R., Wolf, M., Spedding, G.R., Hedenström, A. 2008. Leading-edge vortex improves lift in slow-flying bats. *Science* **319**: 1250-1253. (doi 10.1126/science.1153019)
13. Muijres, F.T., Johansson, L.C., Hedenström, A. 2012 Leading edge vortex in a slow-flying passerine. *Biol. lett.* **8**: 554-557. (doi 10.1098/rsbl.2012.0130)
14. Videler, J.J., Stamhuis, E.J., Povel, G.D.E. 2004 Leading-edge vortex lifts swifts. *Science* **306**: 1960-1962. (doi 10.1126/science.1104682)
15. Usherwood, J.R., Ellington, C.P. 2002 The aerodynamics of revolving wings: I. Model hawkmoth wings. *J. Exp. Biol.* **205**: 1547-1564.
16. Usherwood, J.R., Ellington, C.P. 2002 The aerodynamics of revolving wings: II. Propeller force coefficients from mayfly to quail. *J. Exp. Biol.* **205**: 1565-1576.
17. Usherwood, J.R. 2009 The aerodynamic forces and pressure distribution of a revolving pigeon wing. *Exp. Fluids* **46**: 991-1003. (doi 10.1007/s00348-008-0596-z)
18. Dickson, W.B., Dickinson, M.H. 2004 The effect of advance ratio on the aerodynamics of revolving wings. *J. Exp. Biol.* **207**: 4269-4281. (doi 10.1242/jeb.01266)
19. Lentink, D., Dickinson, M. H. 2009 Rotational accelerations stabilizes leading edge vortices on revolving fly wings. *J. Exp. Biol.* **212**: 2705-2719. (10.1242/jeb.022269)
20. Kruyt, J.W., Quicazán-Rubio, E.M., van Heijst, G.F., Altshuler, D.L., Lentink, D. 2014 Hummingbird wing efficacy depends on aspect ratio and compares with helicopter rotors. *J. R. Soc. Interface* **11**: 20140585. (doi 10.1098/rsif.2014.0585)
21. Han, J.S., Kim, J.K., Chang, J.W., Han, J.H. 2015 An improved quasi-steady aerodynamic model for insect wings that considers movement of the center of pressure. *Bioinspir. Biomim.* **10**: 046014. (doi 10.1088/1748-3190/10/4/046014)
22. Guo, X., Chen, D., Liu, H. 2015 Does a revolving wing stall at low Reynolds numbers?. *Journal of Biomechanical Science and Engineering* **10**: 15-00588. (doi 10.1299/jbse.15-00588)
23. Ellington, C. P. 2006 Insects versus birds: the great divide. In *44th AIAA aerospace sciences meeting and exhibit*, AIAA-2006-35, 450-455.
24. Pitt Ford, C. W., Babinsky, H. 2013 Lift and the leading-edge vortex. *J. Fluid Mech.* **720**: 280-313. (doi 10.1017/jfm.2013.28)
25. Stevens, R. J., Babinsky, H., Manar, F., Mancini, P., Jones, A. R., Granlund, K. O., ... & Gozukara, A. 2016 Low Reynolds number acceleration of flat plate wings at high incidence. In *54th AIAA Aerospace Sciences Meeting*, AIAA 2016-0286. (doi 10.2514/6.2016-0286 )
26. Jones, A. R., Manar, F., Phillips, N., Nakata, T., Bomphrey, R., Ringuette, M. J., ... & Palmer, J. 2016 Leading edge vortex evolution and lift production on rotating wings. In *54th AIAA Aerospace Sciences Meeting*, AIAA 2016-0288. (doi 10.2514/6.2016-0288)
27. Babinsky, H., Stevens, R. J., Jones, A. R., Bernal, L. P., & Ol, M. V. 2016 Low order modelling of lift forces for unsteady pitching and surging wings. In *54th AIAA Aerospace Sciences Meeting*, AIAA 2016-0290. (doi 10.2514/6.2016-0290 )
28. Phillips, N., Knowles, K., Bomphrey, R. J. 2017 Petiolate wings: effects on the leading-edge vortex in flapping flight. *Interface Focus*, **7**: 20160084. (doi 10.1098/rsfs.2016.0084)
29. Lee, Y. J., Lua, K. B., Lim, T. T. 2016 Aspect ratio effects on revolving wings with Rossby number consideration. *Bioinspir. Biomim.* **11**: 056013. (doi 10.1088/1748-3190/11/5/056013)
30. Maxworthy, T. 1979 Experiments on the Weis-Fogh mechanism of lift generation by insects in hovering flight. Part 1. Dynamics of the 'fling'. *J. Fluid Mech.* **93**(01): 47-63.

- 1
  - 2
  - 3
  - 4
  - 5
  - 6
  - 7
  - 8
  - 9
  - 10
  - 11
  - 12
  - 13
  - 14
  - 15
  - 16
  - 17
  - 18
  - 19
  - 20
  - 21
  - 22
  - 23
  - 24
  - 25
  - 26
  - 27
  - 28
  - 29
  - 30
  - 31
  - 32
  - 33
  - 34
  - 35
  - 36
  - 37
  - 38
  - 39
  - 40
  - 41
  - 42
  - 43
  - 44
  - 45
  - 46
  - 47
  - 48
  - 49
  - 50
  - 51
  - 52
  - 53
  - 54
  - 55
  - 56
  - 57
  - 58
  - 59
  - 60
31. McCroskey, W. J. 1981 *The phenomenon of dynamic stall*. NASA Technical Memorandum TM-81264.
32. Ansari, S. A., Żbikowski, R., Knowles, K. 2006 Aerodynamic modelling of insect-like flapping flight for micro air vehicles. *Prog. Aerosp. Sci.* **42**:129-172. (doi 10.1016/j.paerosci.2006.07.001)
33. Kruyt, J. W., van Heijst, G. F., Altshuler, D. L., Lentink, D. 2015 Power reduction and the radial limit of stall delay in revolving wings of different aspect ratio. *J. R. Soc. Interface* **12**: 20150051. (doi 10.1098/rsif.2015.0051)
34. Ormiston, R. A. 2004 Induced power of the helicopter rotor. American Helicopter Society 60th Annual Forum and Technology Display; 8-10 Jun. 2004; Baltimore, MD, 33-53.
35. Chattot, J. J. 2004 Analysis and design of wings and wing/winglet combinations at low speeds. AIAA Paper: AIAA-2004-220.
36. Nabawy, M. R. A., Crowther, W. J. 2014 On the quasi-steady aerodynamics of normal hovering flight part II: model implementation and evaluation. *J. R. Soc. Interface* **11**: 20131197. (doi 10.1098/rsif.2013.1197)
37. Nabawy, M.R.A., Crowther, W.J. 2015 A quasi-steady lifting line theory for insect-like hovering flight. *PloS one* **10**: e0134972. (doi 10.1371/journal.pone.0134972)
38. Nabawy, M.R.A., Crowther, W.J. 2015 Aero-optimum hovering kinematics. *Bioinspir. Biomim.* **10**: 044002. (doi 10.1088/1748-3190/10/4/044002)
39. Deng, X., Schenato, L., Wu, W.C., Sastry, S.S. 2006 Flapping flight for biomimetic robotic insects: Part I-system modeling. *IEEE Transactions on Robotics* **22**: 776-788. (doi: 10.1109/TRO.2006.875480)
40. Berman, G.J., Wang, Z.J. 2007 Energy-minimizing kinematics in hovering insect flight. *J Fluid Mech.* **582**: 153-168. (doi 10.1017/S0022112007006209)
41. Taha, H.E., Hajj, M.R., Beran, P.S. 2014 State-space representation of the unsteady aerodynamics of flapping flight. *Aerosp. Sci. and Technol.* **34**: 1-11. (doi 10.1016/j.ast.2014.01.011)
42. Polhamus, E. C. 1966 A concept of the vortex lift of sharp-edge delta wings based on a leading-edge-suction analogy. NASA Technical Note D-3767.
43. Traub, L. W. 2004 Analysis and estimation of the lift components of hovering insects, *J. Aircraft* **41**, 284-289.
44. Nabawy, M. R. A., Crowther, W. J. 2014 On the quasi-steady aerodynamics of normal hovering flight part I: the induced power factor. *J. R. Soc. Interface* **11**: 20131196. (doi 10.1098/rsif.2013.1196)
45. Ahmed, M. R., Abdelrahman, M. M., ElBayoumi, G. M., ElNomrossy, M. M. 2011 Optimal wing twist distribution for roll control of MAVs. *Aeronaut. J.* **115**, 641- 649.
46. Saffman, P. G., Sheffield, J. S. 1977 Flow over a wing with an attached free vortex. *Studies in Applied Mathematics*, **57**: 107-117.
47. O. Smith, A. M. 1975 High-lift aerodynamics. *J. Aircr.* **12**: 501-530.
48. Harbig, R. R., Sheridan, J., Thompson, M. C. 2013 Relationship between aerodynamic forces, flow structures and wing camber for rotating insect wing planforms. *J. Fluid Mech.* **730**: 52-75. (doi 10.1017/jfm.2013.335)
49. Sane, S. P., Dickinson, M. H. 2002 The aerodynamic effects of wing rotation and a revised quasi-steady model of flapping flight. *J. Exp. Biol.* **205**: 1087-1096.
50. Wang, Z. J. 2005 Dissecting insect flight. *Annu. Rev. Fluid Mech.*, **37**: 183-210. (doi 10.1146/annurev.fluid.36.050802.121940)

- 1  
2  
3  
4  
5  
6  
7  
8  
9  
10  
11  
12  
13  
14  
15  
16  
17  
18  
19  
20  
21  
22  
23  
24  
25  
26  
27  
28  
29  
30  
31  
32  
33  
34  
35  
36  
37  
38  
39  
40  
41  
42  
43  
44  
45  
46  
47  
48  
49  
50  
51  
52  
53  
54  
55  
56  
57  
58  
59  
60
51. Nabawy, M.R.A., Crowther, W.J. Is flapping flight aerodynamically efficient? 32nd AIAA Applied Aerodynamics Conference, AIAA Aviation and Aeronautics Forum and Exposition, 16 - 20 June 2014, Atlanta, Georgia. (doi 10.2514/6.2014-2277 )
  52. Nabawy, M. R., Crowther, W. J. 2016 Optimum hovering wing planform. *J. Theor. Biol.*, **406**: 187-191. (doi 10.1016/j.jtbi.2016.06.024)
  53. Ellington, C.P. 1984 The aerodynamics of hovering insect flight. II. Morphological parameters. *Philos. Trans. R. Soc. Lond. B Biol. Sci.* **305**:17-40. (doi 10.1098/rstb.1984.0050)
  54. Venkata, S.K., Jones, A.R. 2013 Leading-edge vortex structure over multiple revolutions of a rotating wing. *J. Aircraft* **50**:1312-1316. (doi 10.2514/1.C032128)
  55. Polhamus, E. C. 1968 Application of the leading-edge-suction analogy of vortex lift to the drag due to lift of sharp-edge delta wings. NASA Technical Note D-4739.

For Review Only